# EXPERIMENTAL AND NUMERICAL FLOW ANALYSIS OF LOW-SPEED FANS AT HIGHLY LOADED WINDMILLING CONDITIONS

**Aurélie Ortolan***
SAFRAN Technofan
Blagnac, France
Université de Toulouse
ISAE-SUPAERO
Toulouse, France
aurelie.ortolan@isae.fr

**Suk-Kee Courty-Audren**
**Nicolas Binder**
**Xavier Carbonneau**
Université de Toulouse
ISAE-SUPAERO
Toulouse, France

**Florent Challas**
SAFRAN Technofan
Blagnac, France

## ABSTRACT

*This paper aims for the analysis of experimental and numerical results of windmilling flow topologies far from freewheeling condition. Two fans were investigated: a baseline design and an innovative one meant to reach good performance in both compressor and turbine modes. Experiments are conducted with global and local characterizations to determine energy recovery potential and local loss mechanisms. The numerical study is carried out with mixing plane steady simulations, the results of which are in fair agreement with experimental data. The difference of local topology between freewheeling and highly loaded windmill demonstrates that classical deviation rules such as Carter's are not well-suited to highly loaded windmilling flows. Finally, under certain conditions, the minor influence of the stator on the rotor topology indicates that non rotating elements can be considered as loss generators.*

## NOMENCLATURE

**Superscript**

$\hat{\cdot}$ Assessed at the rotor outlet mean quadratic radius

**Subscript**

$\cdot_1$ Inlet
$\cdot_2$ Rotor inlet
$\cdot_3$ Rotor Outlet
$\cdot_9$ Outlet

**Roman symbols**

$P_i$ Absolute total pressure (Pa)
$r$ Radius (m)
$U$ Blade speed (m.s$^{-1}$)
$V$ Absolute velocity (m.s$^{-1}$)
$V_t$ Tangential absolute velocity (m.s$^{-1}$)
$V_x$ Axial absolute velocity (m.s$^{-1}$)

**Greek letters**

$\alpha$ Absolute flow angle (°)
$\beta$ Relative flow angle (°)
$\delta$ Rotor outlet deviation (°)
$\Delta h_i$ Rotor total enthalpy variation (J.kg$^{-1}$)
$\rho$ Density (kg.m$^{-3}$)
$\phi$ Flow coefficient
$\phi_P$ Flow coefficient for the freewheeling operating point
$\hat{\phi}^*$ Reduced flow coefficient
$\psi$ Loading coefficient
$\omega$ Angular blade speed (rad.s$^{-1}$)

**Abreviations**

$FS$ Full scale
$NI$ National instrument

*Address all correspondence to this author.

## INTRODUCTION

In aeronautics, the windmilling phenomenon is described as the spontaneous rotation of a rotor under the effect of a moving fluid. It is generally studied on multistage turbomachineries to assess their relight capabilities and drag in engine-out conditions. Thus, among the different kind of windmilling operation, the freewheeling mode, corresponding to a zero global work through the machine, is the most investigated one in the literature. In this context, windmill is usually considered as a marginal situation of functioning. However, today's aircrafts are becoming more and more "electric". To address this growing need for electrical energy, cooling fans of air systems are regarded as potential energy recovery systems, if operated in load-controlled windmilling.

As previously said, the freewheeling mode of conventional fans has been well documented in the literature. It is characterized by highly negative incidences causing massive separations on both rotor and stator ([1]). In addition, a mixed local behaviour along the rotor blade is generally recorded: energy-giving zone near the hub and energy-extracting zone near the shroud. Only the position of the neutral radius differs between studies and seems to depend mainly on the fan geometry ([2–4]). The present study is interested in the evolution of the topology from freewheeling mode to highly loaded windmilling condition. The literature, although essentially focused on comparing the flow topology at freewindmill with that of the design point, gives some important results within the scope of this paper. In particular, at freewindmill, the rotor outlet deviation seems to be generally small ([2]) and well-predicted by the Carter's rule ([4]). Prasad and Lord numerically investigated several freewheeling conditions (corresponding to several massflows) and demonstrate that the rotor outlet deviation remains unchanged. Expressed with adimensionalized parameters, it means that the flow topology is the same at a given value of flow coefficient [5].

The influence of the stator on the rotor flow topology also has to be underlined. The rotor performance at the freewindmill seems to be influenced by the nature of the flow in the stator ([2]). The blockage occurring in the latter, due to massive separation, modifies the radial distribution of axial velocity, leading to high values near the hub, as observed in [6]. According to [2], the signature of this distortion is observed upstream, up to the rotor plane. But the results presented in the paper show a strong attenuation and the actual significance of this distortion could be discussed. It will be shown that the present work leads to the opposite conclusion, with comparable distance between the rotor and the stator (the information about the distance between the rotor an the stator is not explicitly mentioned in [2] and is estimated from the illustration proposed).

Regarding the numerical predictivity in freewheeling conditions, it appears that global performances are generally well assessed by the simulations whereas some differences remain locally on the blade passage ([2]). However, some studies show that numerically imposing the inlet distorsion recorded during the tests (instead of setting uniform inlet boundary conditions) has a corrective effect on the local topology ([1,5]).

The scope of the present paper is to bring some new elements about windmilling flows by focusing on highly loaded cases, where little information is available. Two major fans are investigated in this study: a baseline design, only conceived to work as a compressor, and an optimized fan, meant to reach good efficiency in both compressor and turbine mode (windmilling). Their global performance and local topology were numerically investigated in a previous study of the present authors ([7]). With only numerical data, it led to the conclusion that the innovative design was able to operate satisfactorily in antagonist functioning modes, in accordance with its original purpose.

In this paper, three major topics are investigated:

- Numerical results are confronted to experimental data for the conventional fan and the optimized design.
- The effect of the stator on the rotor flow is tackled on an experimental point of view. To this end, the rotor of each machine (conventional fan and optimized design) is tested with its own stator and with that of the other fan.
- The local topology at highly loaded windmill is experimentally compared with that of freewindmill, for the two main machines. The nature of the flow is suspected to be highly different and this study aims at proving this hypothesis.

## MACHINES AND OPERATING RANGES

The machines investigated in this paper are axial fans of rotor-stator type. The conventional fan was designed for a given massflow and pressure ratio. For the optimized geometry, this performance had to be reached while preserving the same diameter (limited by the size of the vein) and drastically increasing the efficiency target in load-controlled windmilling. Such a non-conventional stage implies a non-conventional design process such as the one described in [7]. Thus, the design point is not the adequate reference for a comparison between the stages. Speaking of windmilling operation, [5] underlines the relevance of the freewindmilling flow coefficient $\hat{\phi}_P$ as a key parameter of the problem. For the conventional fan, $\hat{\phi}_P = 0.946$, and for the optimized one, $\hat{\phi}_P = 0.496$. This difference illustrates the fact that the non-conventional design requires high rotational speeds.

Figures 1 and 2 show a blade-to-blade view of the stage of the two main geometries, referred as R1S1 (baseline design) and R2S2 (optimized design) configurations. "Hybrid" configurations are also tested: Rotor 1 and Stator 2, Rotor 2 and Stator 1. The rotor/stator distance is about 0.65 of rotor chord for all fans. The illustrations of Figs. 1 and 2 are only schematic, since the geometry of the two machines is confidential. The R2S2 fan differs from the R1S1 one both in terms of rotor and stator geometry. The rotor was entirely modified (camber, metal angles, chord) to be able to give and extract work to the fluid according to the considered mode (compressor or turbine). Classical sta-

tors (such as Stator 1) in windmilling operation are reported to be highly separated due to a poor adaptation of the flow. Consequently, a variable camber stator was imagined to locally align the leading edge to the direction of the flow in both compressor and turbine mode. The mechanical realisation and the feasibility study of such a solution is currently ongoing. [1] For the experiment, a set of fixed-geometry devices is used in order to check the aerodynamic relevance and performance of the concept.


**FIGURE 1**. R1S1 AN R1S2 CHARACTERISTICS.


**FIGURE 2**. R2S2 AN R2S1 CHARACTERISTICS.

In this paper, in order to describe the overall performance of the studied fans, a loading-to-flow-coefficient diagram is used. This formalism is suitable to off-design configurations as reported in [8]. These global parameters are defined thanks to a reference radius, namely the quadratic mean of hub and shroud radii, assessed at the rotor oulet:

$$\begin{cases} \hat{\psi} = \dfrac{\Delta h_{i23}}{\hat{U}^2} & (1) \\ \hat{\phi} = \dfrac{V_{x2}}{\hat{U}} & (2) \\ \hat{r} = \sqrt{\dfrac{r_{shroud}^2 + r_{hub}^2}{2}} & (3) \\ \hat{U} = \omega \hat{r} & (4) \end{cases}$$

However, as one of the objectives of this paper is to compare several fan geometries, an additional parameter has to be introduced: the reduced flow coefficient $\hat{\phi}^*$ expressed as:

$$\hat{\phi}^* = \frac{\hat{\phi}}{\hat{\phi}_P} \quad (5)$$

[1] A fall-back solution would be a fixed stator with zero stagger angle. This was numerically tested and shows good results since a maximum efficiency of 0.70 was obtained in both compressor and turbine modes.

In Eqn. 5, $\hat{\phi}_P$ corresponds to the freewindmilling flow coefficient aforementioned. This parameter, depending on the rotor geometry (and on possible inlet distortions), is recalled for R1S1 and R2S2 fans: respectively equal to $\hat{\phi}_P = 0.946$ and $\hat{\phi}_P = 0.496$. The freewheeling condition is thus reached for $\hat{\phi}^* = 1$, for which zero global work is recorded through the machine. Compressor and turbine modes are respectively characterized by $\hat{\phi}^* < 1$ and $\hat{\phi}^* > 1$. The windmilling operating ranges of the two machines in terms of flow coefficient $\hat{\phi}$ are therefore totally different. The reduced parameter $\hat{\phi}^*$ is used to compare different machines for an equivalent incursion in load-controlled windmilling operation. An illustration of the velocity diagrams for all machines is given on Fig. 3.

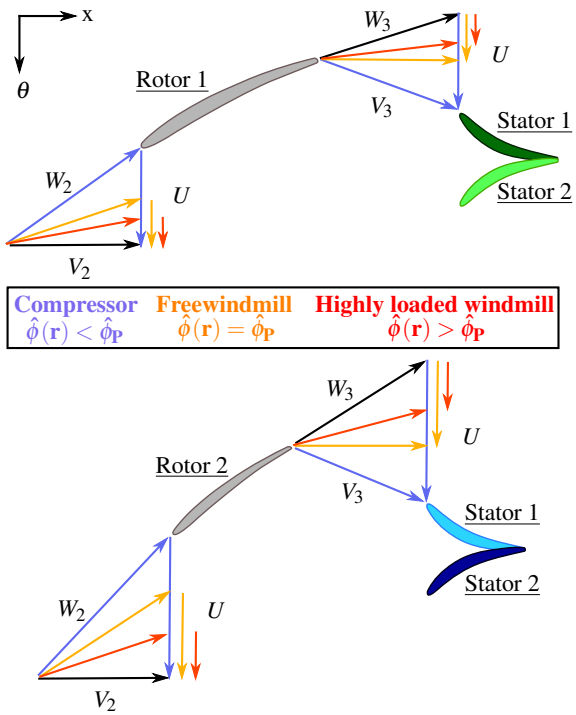


**FIGURE 3**. VELOCITY DIAGRAMS FROM COMPRESSOR TO TURBINE MODE.

## EXPERIMENTAL SET UP

The experimental study is carried out in the Department of Aerodynamics, Energetics and Propulsion (DAEP) of ISAE-SUPAERO. A test facility has been recently developed, dedicated to the windmilling of low-dimension fans (diameter $\leq$ 200mm). A dual management of the energy (air vacuum system and asynchronous electrical engine) allows the independent setting of flow generation and shaft loading. The latter and the rotational speed are measured and controlled by the differential transformer torque meter (Magtrol TM 306) coupled with the electrical en-

gine. Thanks to this regulation system, a complete exploration of the operating line is possible: from surge limit to locked rotor configuration. To protect the measurements from electromagnetic disturbance, the engine is deported far from the test section. The latter is reversible to invert the flow direction, if required. Fan geometries consist of fixed removable rotors and stators. Both global and local measurements are implemented

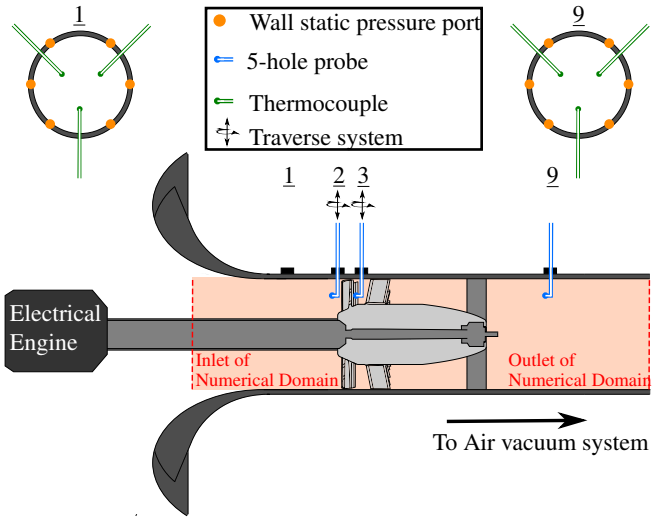


**FIGURE 4**. ILLUSTRATION OF THE DAEP WINDMILLING TEST FACILITY AND THE NUMERICAL DOMAIN (ORANGE).

to quantify the power recovery and to study the flow topology around the rotor. The test rig, illustrated in Fig. 4, is divided in two parts: a calibrated bell mouth that assesses the massflow through the vein and the instrumented test section. Global characterizations are located at inlet (Plane 1) and outlet (Plane 9) and consist of 3 thermocouples (Type K, basic accuracy 1°) and a 6-hole Kent chamber connected to a differential sensor (Rosemount, 0/100mbars, basic accuracy 0.15% FS). This enables to measure the mean total temperature and the mean static pressure. In addition, the outlet (plane 9) is equipped with a fixed five-hole probe used to get the total pressure (Keller, $-150/+100$mbars, basic accuracy 0.047% FS). As for the local characterizations, two directionnal five-hole probes are located 7 mm upstream the leading edge and 5 mm downstream the trailing edge of the rotor (Keller, $-150/+100$mbars, basic accuracy 0.047% FS, Rosemount $-50/50$mbars, basic accuracy 0.15% FS). The radial probing of velocity field and pressure is conducted from hub to shroud through around 35 positions. Data acquisition is achieved by a composite NI cDAQ-9172 device connected to 3 kind of NI modules that are used for current (NI 9215), voltage (NI 9203) and temperature (NI 9211) recordings. The measurements were acquired on 5000 samples with a sampling frequency of 20kHz.

Experimentally, four rotor/stator configurations were tested: Rotor 1 and Stator 1 (R1S1), Rotor 2 and Stator 2 (R2S2), Rotor 1 and Stator 2 (R1S2), Rotor 2 and Stator 1 (R2S1). The last two cases enable to check the extent to which the stator influences the rotor topology. As for global performances, a large operating range in windmilling conditions was explored in order to obtain the loading to flow coefficient diagram. As for the local topology, two particular operating points were emphasized. The first one corresponds to the freewheeling condition and is reached when the shaft torque is equal to zero. This point was obtained for a rotational speed of 2500rpm for R1S1 and 3900rpm for R2S2. The second one was chosen at highly loaded windmill, for the reduced flow coefficient $\hat{\phi}^* = 3$. It corresponds to a rotational speed of 1300rpm for R1S1 and 3000rpm for R2S2.

## NUMERICAL SET UP

The numerical domain is illustrated in Fig. 4. The shaft, the bell mouth and the rear support, present on the experimental facility, are not numerically represented. The domain is discretized with a multi-block structured mesh generated with AutoGrid 5$^{TM}$, a module of FINE$^{TM}$/Turbo (CFD suite of Numeca). The mesh consists of O-grid blocks located around the blades, and H-grid blocks in the passage (O4H mesh). The overall mesh size, previously tested according to the objectives of this study, is 1.5M pts with 0.7M pts in the rotor and 0.4M pts in the stator for both fans. The first cell at the wall was set to 10 $\mu$m. The mean value of the $y^+$ parameter at walls is about 1.6 ($y^+_{max} \approx 8$) for all computations.

A three-dimensional finite-volume Navier-Stokes solver was used for the mixing plane steady simulations. They were performed with the Euranus solver of FINE$^{TM}$/Turbo V9.0.2. Time discretization is ensured by a four-stage Runge-Kutta scheme. Local-time stepping and a three-level multigrid technique are used to accelerate the convergence. The discretization in space is based on a cell-centered finite-volume approach. Convective fluxes are determined by a Jameson second-order centered scheme with added artificial dissipation. Uniform absolute total pressure and temperature were imposed at the inlet. At the outlet, the massflow was imposed with pressure adaptation. As for the turbulence closure, the two-equation SST model was used. In agreement with the NUMECA documentation ([9]), the turbulence intensity was calculated based on the Reynolds number and is contained between 3% (for the highest flow coefficients) and 4% (for the smallest flow coefficients).

The computations were carried out for only R1S1 and R2S2 configurations. Several values of massflow and speed lines (from 8000 to 20000rpm) are simulated from compressor surge to turbine blockage. This was used, among other things, to plot the numerical loading-to-flow-coefficient diagram. For this paper purposes, extra simulations were done on the two experimental operating points described above ($\hat{\phi}^* = 1$ and $\hat{\phi}^* = 3$).

## RESULTS ANALYSIS

In this section, the numerical and experimental results for the four fans configurations tested are presented and analyzed according to the three major subjects tackled in this paper.

### Numerical validation

In this part, numerical and experimental trends are confronted on global and local point of view.

**Global performance.** Figure 5 shows the numerical and experimental loading-to-reduced flow coefficient diagrams for R1S1 and R2S2 configurations. Theoretically, the reduction of the flow coefficient $\hat{\phi}$ by its neutral value, $\hat{\phi}_P$, makes the $(\hat{\phi}^*, \hat{\psi})$ characteristics of R1S1 and R2S2 configurations collapse. This result is confirmed by numerical $(\hat{\phi}^*, \hat{\psi})$ lines for positive values of $\hat{\psi}$ (compressor mode). For both machines, a slope break is observed between the compressor ($\hat{\phi}^* < 1$) and turbine ($\hat{\phi}^* > 1$) modes. This can probably be related to the non linear evolution of the rotor outlet deviation with the reduced flow coefficient in turbine mode. This point is suspected because of the massive separation that occurs in windmilling operation. The experimental data confirmed the numerical trend in turbine mode and demonstrate that the value of the slope in this region is depending on the rotor geometry.

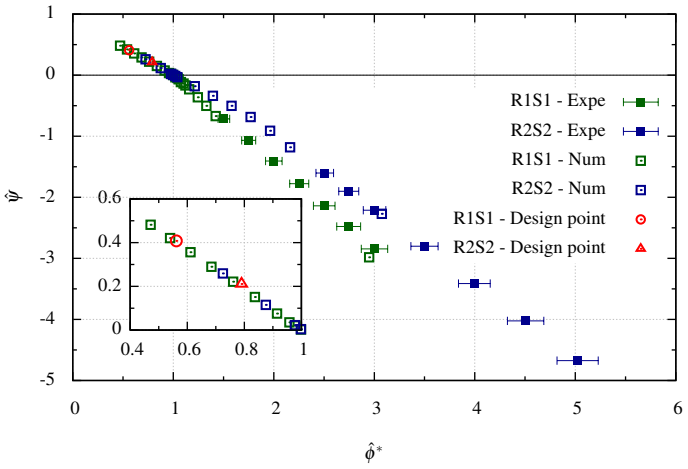


**FIGURE 5**. EXPERIMENTAL AND NUMERICAL LOADING TO REDUCED FLOW COEFFICIENT DIAGRAM FOR R1S1 AND R2S2 CONFIGURATIONS.

**Local topology.** The radial work distribution is numerically and experimentally presented in Fig. 6 for the freewheeling condition and for highly loaded windmill. At $\hat{\phi}^* = 1$, the numerical results well match the experimental data for both fans. At $\hat{\phi}^* = 3$, for R2S2 configuration, the radial distribution is relatively well predicted by the simulations, especially in the region corresponding to the tip leakage (from $h/H = 75\%$ to shroud). A non negligeable offset is however visible in the remaining blade span. For R1S1 configuration, at the same loaded conditions, the numerical distribution does not reproduce the irregular shape recorded by the experiment. Nevertheless, mean values of work exchange are in fair agreement with measurements. The same behaviour is also observed on the rotor total pressure variation as discussed below.

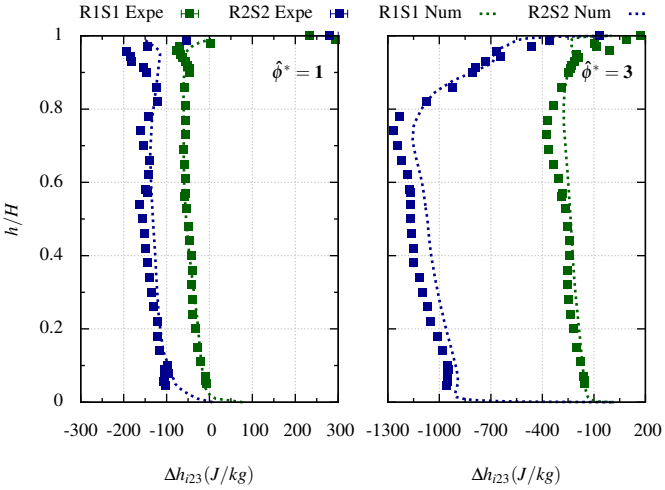


**FIGURE 6**. EXPERIMENTAL AND NUMERICAL RADIAL WORK DISTRIBUTION FOR R1S1 AND R2S2 CONFIGURATIONS.

Figure 7 shows the radial distribution of the rotor total pressure variation for R1S1 and R2S2 configurations. In freewheeling condition, the distribution is well predicted for R2S2 but far less for R1S1. The biggest differences are observed in regions where massive separations are expected. It seems that the numerical approach underestimates the stall intensity. This may come from different possible origins: under refined mesh, turbulence modelling, RANS approach. Yet, the mesh size of this study is similar to the one used by Gill ([6]). The same observation can be done for this geometry at $\hat{\phi}^* = 3$. However, as regards R2S2 configuration at highly loaded windmill, discrepancies begin to occur in the upper half of the blade span. The same causes (mesh under refinement) are suspected.

Overall, the numerical prediction is good as far as the global performances are concerned. The local prediction capabilities need to be improved. Numerical simulations inaccurately estimate local variations in stalled regions and tip leakage flow areas, which is not unusual with RANS approach. However, mean values are reasonably well captured by calculations.

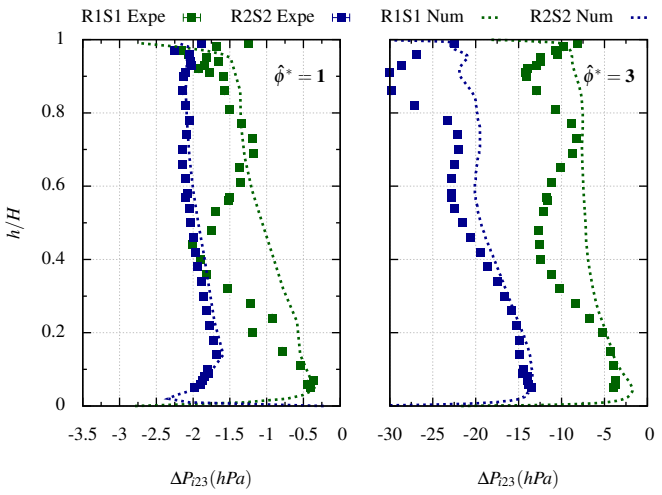


**FIGURE 7**. EXPERIMENTAL AND NUMERICAL ROTOR ABSOLUTE TOTAL PRESSURE VARIATION FOR R1S1 AND R2S2 CONFIGURATIONS.

### Influence of the stator on the rotor topology

The effect of the stator is experimentally investigated on both global and local results at $\hat{\phi}^* = 3$. The classical rotor and the optimized one are coupled with a conventional stator (Stator 1) that generates great losses in windmilling operation and an optimized stator (Stator 2) expected to be far less separated.

**Global performance.** Experimental $(\hat{\phi}^*, \hat{\psi})$ evolutions are reported in Fig. 8 for the four geometries.

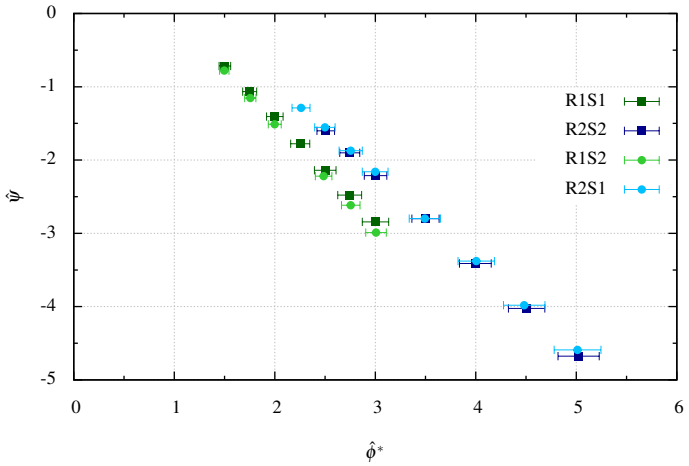


**FIGURE 8**. EXPERIMENTAL LOADING TO REDUCED FLOW COEFFICIENT DIAGRAM FOR THE FOUR MACHINES.

Mainly two evolutions are visible on this graph. R1S1 and R1S2 configurations characteristics are very close and R2S2 and R2S1 configurations lines are almost the same. As the theoretical trends are given by the absolute flow angle at rotor inlet $\alpha_2$ and the relative flow angle at rotor outlet $\beta_3$ ([10]), this result suggests that these two angles are barely affected by the stator geometry. A closer look emphases some differences between R1S1 and R1S2 configurations characteristics, the latter having a steeper slope.

**Global stator losses.** Figure 9 gives an insight of the adimensionalized stator losses evolution with the massflow for the rotor 2 combined with either Stator 2 or Stator 1 (respectively R2S2 and R2S1 configurations). The data were measured at the mean quadratic radius. As expected, the use of a conventional stator in highly loaded windmilling conditions leads to higher losses. For each geometry, the rotor outlet absolute angle at this given radius is highly negative. This means that the incidence corresponding to a perfect adaptation of the flow at the stator inlet is never reached.

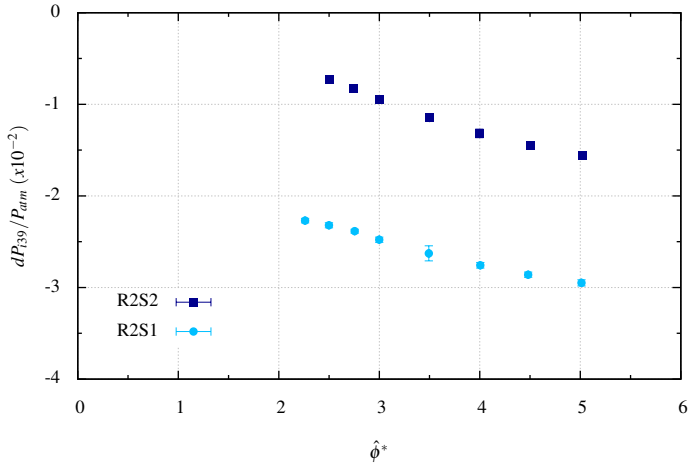


**FIGURE 9**. EXPERIMENTAL STATOR ABSOLUTE TOTAL PRESSURE VARIATION FOR R2S2 AND R2S1 CONFIGURATIONS.

**Rotor outlet Axial velocity** Experimental radial profiles of the axial velocity at the rotor outlet are presented in Fig. 10 for the four machines tested. As can be seen, the geometries with the stator suitable for windmilling operation (Stator 2) are characterized by higher values of axial velocity from hub to shroud. This means that for the same air vacuum configuration, the massflow is higher, confirming the reduction of the vein blockage, due to the massive separation recorded in stator 1. In addition, the profiles of axial velocity, adimensionalized by its mean value, overlap for a given rotor, as visible in Fig. 10. This

demonstrates that radial distribution of this parameter is only depending on the rotor geometry for a given value of global reduced flow coefficient. The linear decrease with blade span recorded for R2S2 and R2S1 configurations can be related to the local acceleration around the bulb (hub) and the radial work distribution.

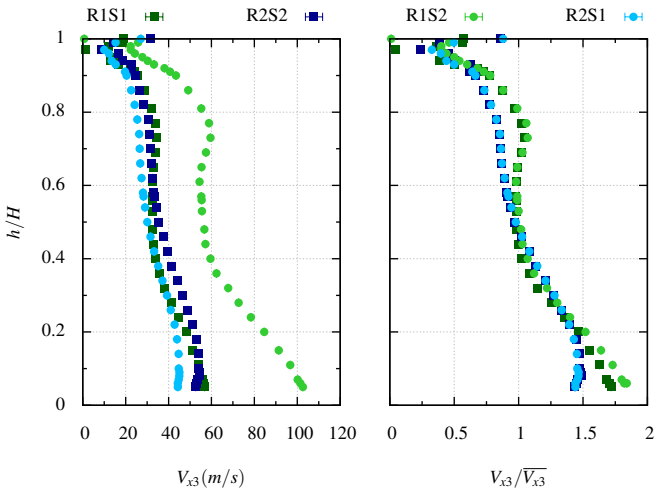


**FIGURE 10**. EXPERIMENTAL AXIAL VELOCITY PROFILES AT ROTOR OUTLET FOR THE FOUR MACHINES.

**Rotor outlet deviation.** The effect of the stator row on the relative flow angle at the rotor outlet is small. This result is presented in Fig. 11 in terms of deviation, which is not affected by the change of the stator.

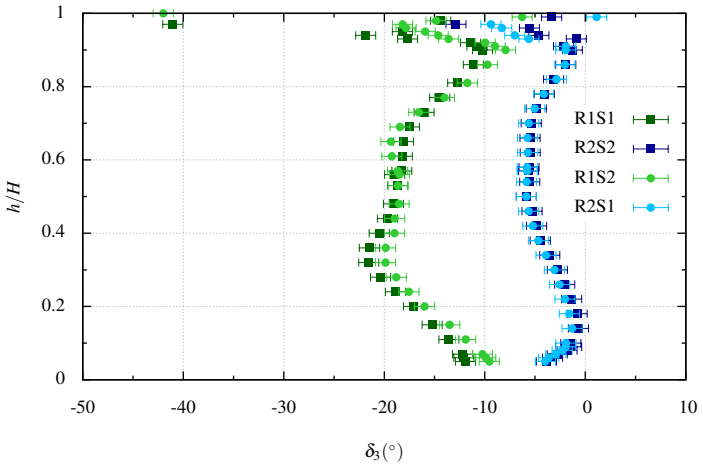


**FIGURE 11**. EXPERIMENTAL ROTOR OUTLET DEVIATION FOR THE FOUR MACHINES.

The greatest discrepancy is observed between R1S1 and R1S2 configurations but is inferior to measurement uncertainties. As the axial velocity and the outlet deviation at rotor outlet are little dependant on the stator geometry, it means that the absolute angle at stator inlet is only influenced by the global flow coefficient. The stator blades angles must be adapted to suit the local direction of the flow.

**Rotor Outlet loading coefficient.** Beyond axial velocity and flow angle, the effect of the stator is analysed in terms of local loading coefficient (Fig. 12). Small influence of the stator on the rotor loading coefficient for R2S2 and R2S1 configurations is reported. On the contrary some differences are visible between R1S1 and R1S2 configurations for $h/H \in [0.2, 0.8]$ even if general shape is preserved. Loading coefficient is more negative for R1S2 than for R1S1. This result confirms the small differences pointed out in Fig. 8, where the global loading coefficient of R1S2 configuration was inferior to that of R1S1 configuration. The irregular distribution of this parameter with the radius in this region is reported to result from massive separation on the pressure side of the blade.

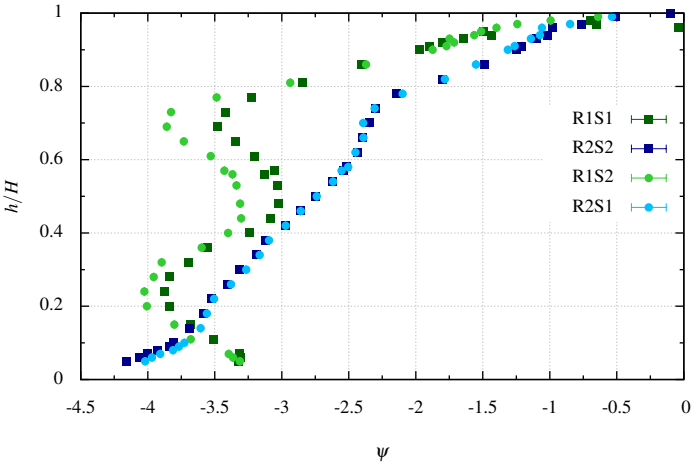


**FIGURE 12**. EXPERIMENTAL LOADING COEFFICIENT FOR THE FOUR MACHINES.

Entropy contours at rotor outlet are given Figs. 13 and 14 for R1S1 and R2S2 configurations respectively at $\hat{\phi}^* = 3$. Even if the local topology of the numerical model is not strictly validated, it gives interesting qualitative information. Tip leakage flow is responsible for most of the entropy creation for R2S2 configuration whereas for R1S1 configuration tip leakage flow and massive separation in the rotor equally contributes at the loss creation. Rotor 1 is characterized by greater loading coefficient and greater camber. This may cause more pronounced adverse pressure gradients and bigger separation.

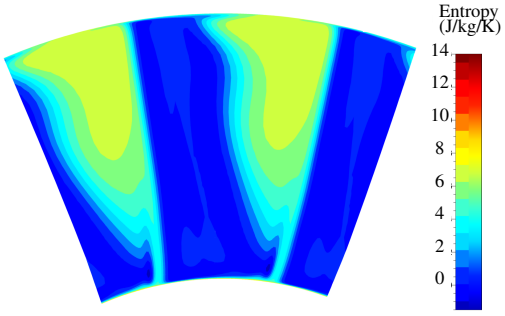


**FIGURE 13**. COMPUTED ENTROPY CONTOURS AT THE ROTOR OUTLET FOR R1S1 CONFIGURATION.

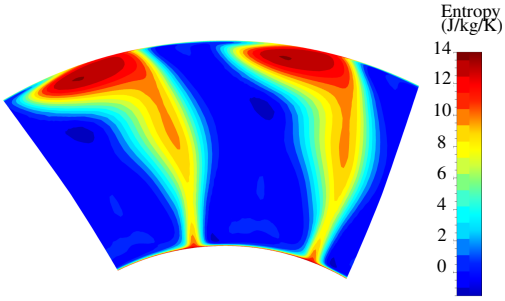


**FIGURE 14**. COMPUTED ENTROPY CONTOURS AT THE ROTOR OUTLET FOR R2S2 CONFIGURATION.

It is found that global and local variations of loading coefficient are weakly affected by the change of stator. Local flow topology at rotor outlet (reduced axial velocity $V_{x3}/\overline{V_{x3}}$ and deviation $\delta_3$) remains unchanged by stator modifications. On the contrary, losses are significantly decreased by the use of stator adapted to power generation (Stator 2). The radial distortions of rotor outlet axial velocities, and especially the high values recorded near the hub, turn out to come from a blockage in the rotor passage, due to massive separations and intense tip leakage flows. The rotor axial velocity distributions are therefore only imputed to rotor topology. This is not in accordance with the conclusions presented in [2], where such a distortion is imputed to the influence of the stator. This specific point has already been discussed in the introduction. But the present results reinforce our perception of weak coupling between the rotor and the stator. A sensitivity analysis of this coupling must be extended to geometric parameters, such as hub-to-tip ratio, or operating parameters, such as the Mach number, for a formal generalization. But it is guessed that the leading parameter of the problem is the axial distance between the rotor and the stator, which is generally small for cooling fans applications ($\approx$ 1 chord), compared with turbofan geometries ($\approx$ 2 to 3 chord). In a system approach, the stator could be considered as a loss generator, which interferes with the overall permeability of the system. The rotor flow will then fit the mass flow imposed by the permeability, according to the loading of the shaft, as described in [5].

## Comparison of flow topology at freewindmill and highly loaded windmill

In this section, the experimental local topology of the two main geometries (R1S1 and R2S2 configurations) is compared for two turbine operating points: the freewheeling condition and a highly loaded windmilling point.

**Rotor outlet deviation.** Figures 15 and 16 present the radial distribution of rotor outlet deviation for R1S1 and R2S2 configurations respectively, at the two aforementioned operating points. The deviation predicted by the carter's law is also plotted. It can be seen that the deviation is greater for the conventional fan than for the optimized one in each case. This result was expected because of the small camber of the new rotor. In freewheeling condition, deviation predicted by Carter's rule is in good agreement with experimental results of R2S2 configuration, which is not so obvious for R1S1 configuration ($\delta_{Carter} \approx -5°$ and $\delta_{Expe} \approx -10°$). Yet, the literature seems to recommend the use of the Carter's rule to approximate the deviation of conventional fans at freewheeling condition ([4]). The present result moderates this remark since it depends on the fan geometry.

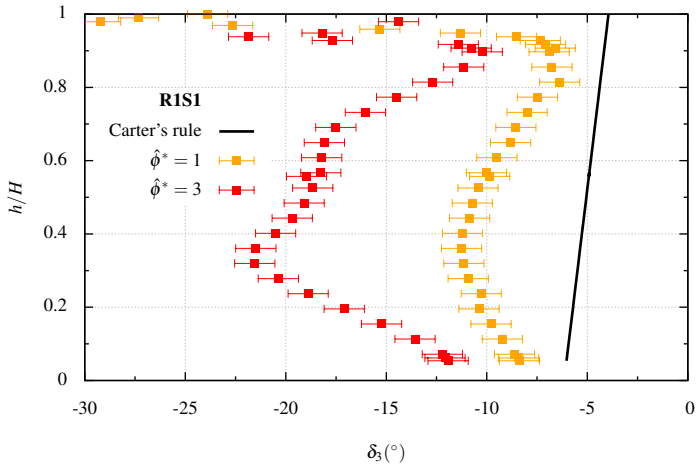


**FIGURE 15**. EXPERIMENTAL ROTOR OUTLET DEVIATION FOR R1S1 CONFIGURATION VS CARTER'S DEVIATION.

At highly loaded windmill, whatever fan considered, the radial profile of the deviation is less regular along the blade. The higher the operating point in turbine mode, the wider the flow is separated in the conventional fan design. This is responsible for a radial deformation of the deviation profile. The deviation outlet angle is influenced by the local loading of the blade (Kutta-Joukowski condition at the trailing edge) which depends on blade camber and operating point, as dicussed in [10]. As R2S2 configuration is more suitable for loaded windmilling operation, the flow is less separated than for R1S1 configuration,

hence the more regular curve obtained at $\hat{\phi}^* = 3$. At any rate, in far off-design conditions, the deviation modelling by a linear law such as Carter's is not appropriate anymore.

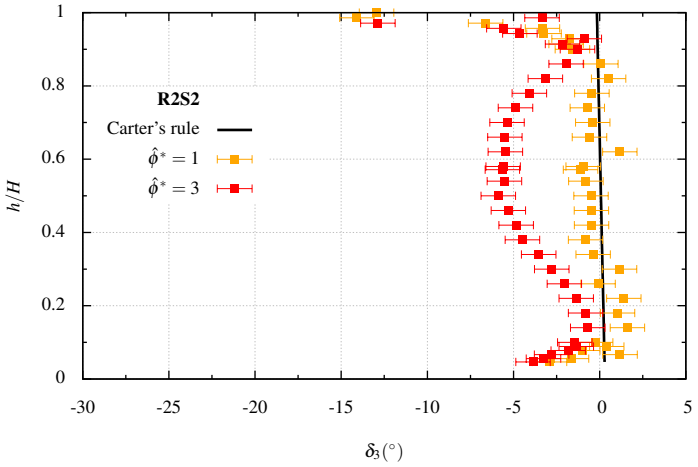


**FIGURE 16**. EXPERIMENTAL ROTOR OUTLET DEVIATION FOR R2S2 CONFIGURATION VS CARTER'S DEVIATION.

**Total enthalpy radial distribution.** Figures 17 and 18 show the experimental total enthalpy variation for the same geometries and operating points as before. This parameter was calculated from the difference of the product $U(r)Vt(r)$, given by the profiles extracted from the 5-hole probes located upstream and downstream of the rotor.

At $\hat{\phi}^* = 3$, these figures show that R2S2 configuration is more suitable for turbine operation since the work exchange is five times higher than for R1S1 configuration. At $\hat{\phi}^* = 1$, a local co-existence of compressor (near the hub) and turbine (near the shroud) modes is recorded for the R1S1 machine (conventional fan), as mentioned in [2–5]. As for the R2S2 configuration, a more complex behaviour appears since the outboard sections of the blade near the shroud are characterized by a compressor zone. Actually, according to the Rotor 2 design, the radial work distribution was expected to be constant and centered around zero. This point still needs more investigation. At highly loaded windmill, in both cases, the work extracted is altered near the shroud from 75% of the blade span due to the tip leakage flow. The proportion of the vein affected by this secondary flows is found to be more important in loaded conditions. For the R1S1 configuration, the decrease in velocity near the shroud is such that it causes the local flow coefficient $\phi$ to drop below the local value of $\phi_P$ ([5]), leading to a stirrer behaviour. The subfigure in Fig. 17 confirms this result. On this graph, two curves are visible. The first one corresponds to the outlet total pressure divided by the inlet total pressure. The second one shows the work contribution to the pressure which is added to the inlet total pressure (in an incompressible approximation). The difference between the two curves represents the losses through the rotor. Near the shroud, above 95% of the blade span, a positive work is recorded whereas the overall $Pi_3/Pi_2$ ratio shows a relaxation, hence the observed "stirrer" zone. This result was sensed in a previous study by Binder ([5]). The author theoretically introduced the possible existence of a stirrer region near the shroud due to local decrease in the flow coefficient. The lack of experimental data in the shroud nearest region didn't enable to confirm this intuition, unlike the experimental results presented in this section.

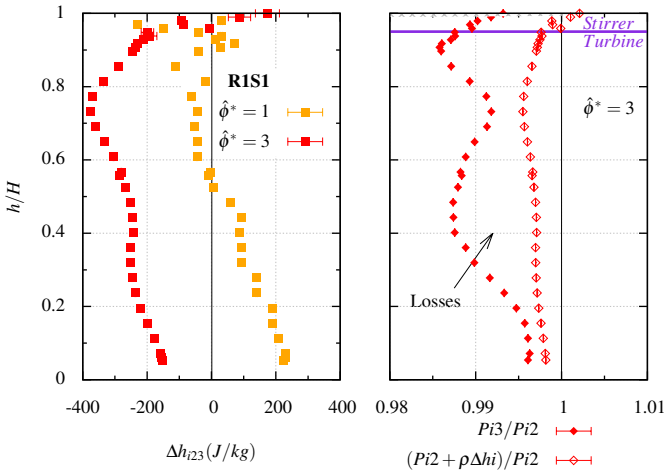


**FIGURE 17**. EXPERIMENTAL WORK AND LOSSES DISTRIBUTIONS FOR R1S1 CONFIGURATION.

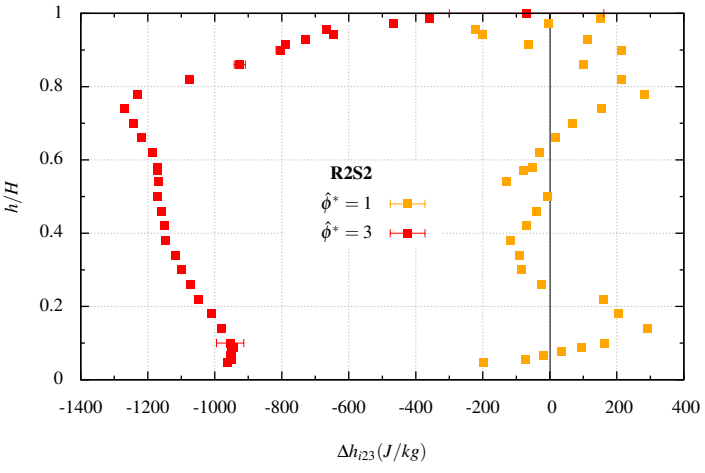


**FIGURE 18**. EXPERIMENTAL WORK DISTRIBUTION FOR R2S2 CONFIGURATION.

Experimental results show that local topology at highly loaded windmill differs from that of freewheelling conditions. Accuracy of classical deviation rules start to worsen in loaded conditions mainly due to massive separations which alter the linearity of relative flow angle variations. Rotor work exchange is far more important for R2S2 than for R1S1 fan, at the same reduced flow coefficient, attesting the improvement of the new design. Loaded windmill conditions are characterized by stronger tip leakage flows which decrease power recovery of the blade tip.

## CONCLUSION

In this paper, numerical predictivity in freewheeling and highly loaded windmill is investigated. The influence of the stator on the rotor global performance and local topology is also discussed. Finally, the evolutions of the flow properties from freewheeling to loaded windmill are analysed. Main findings can be summarized as follows:

- Global and local predictivities of RANS mixing plane steady simulations are good near freewindmill. At highly loaded windmill, mean values of radial distributions of work and rotor total pressure variations are fairly estimated but local discrepancies appear in stalled and tip leakage regions.
- Global performances and the local rotor topologies are hardly affected by the change of stator. Stator modifications strongly alter losses in non rotating rows. Results show that stators designed for compressor functioning generate greater losses in windmilling than those optimised for turbine operation. An exhaustive parametric study is required for a formal generalization of these results, but it is guessed that the axial distance between rotor and stator is the key parameter to the coupling between those two rows. The present distance, typical of cooling fans (about 0.65 of the rotor chord), is far smaller than the one observed on typical turbofans. Similar conclusions are thus expected for those applications. As a consequence, in the prospect of system level resolution, the stator could be considered as a loss generator, which contributes to the overall permeability of the system.
- The increase in reduced flow coefficient leads to more irregular radial distributions due to more separated flow regions and wider tip leakage flow. Thus, classical deviation rules are not appropriate any more in highly loaded windmill.

## PERSPECTIVE

Future work will focus on :

- Explaining the numerical/experimental discrepancies at highly loaded windmill.
- Explaining the influence of the stator on global and local loading coefficient for R1S1 configuration.
- Defining experimental rotor outlet deviation laws for highly loaded windmill.
- Understanding the work distribution for R2S2 configuration.
- Taking into account the compressibility effects.

## ACKNOWLEDGMENT

This study was performed within the scope of the CORAC GENOME project, which aims at optimizing the power management in more electric aircrafts. The authors would like to thank the CORAC consortium, created on the government initiative to harmonize the research efforts in aeronautics. The authors are also grateful to the technical staff without whom the experimental study presented in this paper wouldn't have occurred in time.

## REFERENCES

[1] Courty-Audren, S.-K., 2015. "Identification et compréhension des mécanismes aérodynamiques liés au potentiel de récupération d'énergie. Application à un ventilateur axial subsonique en autorotation". PhD thesis, ISAE-SUPAERO.

[2] Gunn, E. J. and Hall, C. A., 2015. "Loss and deviation in windmilling fans". In Proceedings of *the 11th European Conference on Turbomachinery*, March 23-27, Madrid, Spain. ETC2015-061.

[3] Garcia Rosa, N., Pilet, J., Lecordix, J.-L., Barenes, R. and Lavergne, G., 2013. "Experimental analysis of the flow through the fan stage of a high-bypass turbofan in windmilling conditions". In Proceedings of *the 10th European Conference on Turbomachinery*, April 15-19, Lappeenranta, Finland. ETC2013-162.

[4] Prasad, D. and Lord, W. K., 2010. "Internal losses and flow behavior of a turbofan stage at windmill". *Journal of Turbomachinery,* ***132***(3), pp. 031007–10.

[5] Binder, N., Courty-Audren, S.-K., Duplaa, S., Dufour, G. and Carbonneau, X., 2015. "Theoretical analysis of the aerodynamics of low-speed fans in free and load-controlled windmilling operation". *Journal of Turbomachinery,* ***137***(10), pp. 101001–12.

[6] Gill, A., 2011. "Four quadrant axial flow compressor performance". PhD thesis, Stellenbosch University.

[7] Ortolan, A., Carbonneau, X., Binder, N., Challas, F. and Meauze, G., 2015. "Innovative fan design for both high compressor and windmilling performance". In Proceedings of *the 12th International Symposium on Experimental and Computational Aerothermodynamics of Internal Flows*, July 13-16, Lerici, Italy. ISAIF12-068.

[8] Turner, R. C. and Sparkes, D. W., 1963. "Complete characteristics for a single stage axial flow fan". In Proceedings of *the Institution of Mechanical Engineers*, **178**(9), pp. 14–27.

[9] NUMECA, 2013. *User Manual FINE$^{TM}$/Turbo v.9.0.2*. Brussels, Belgium, August.

[10] Cumpsty, N. A., 2004. *Compressor aerodynamics*. Krieger.